International Journal Multidisciplinary
Homepage : https://journal.antispublisher.com/index.php/IJMI
Email : admin@antispublisher.com

e-ISSN : 3031-9870
IJMI, Vol. 3, No. 1, February 2026
Page 1-15

The investigation of the Effect of Axial Force on Deformation of a bent tube

Hassan Raheem Hassan
Al-Shatrah University, Iraq

DOI : https://doi.org/10.61796/ijmi.v3i1.381

Sections Info

Article history:
Submitted: June 30, 2025
Final Revised: July 07, 2025
Accepted: July 21, 2025
Published: August 16, 2025

Keywords:
Rotary draw bending
Additional tensile
Neutral axis shifting
Finite element analysis

ABSTRACT

Objective: *The inquiry may yield evidence regarding the impact of tension force on the displacement of the neutral axis, strain, and wall thickness in rotary draw bending.* ***Method:*** *The finite element analysis use the ABAQUS software to evaluate the non-linear response of structures.* ***Results:*** *The simulation results align closely with the experimental findings, and we also compared the effects of rotary draw bending with and without axial force, as discussed in previous work without axial force.* ***Novelty:*** *The tube diameter, wall thickness, bending radius, material characteristics, and bending angle are the primary parameters influencing the change of neutral axis shifting and the tensile force in the tube. The neutral axis at the center of the tube shifts to the inner arc due to the additional axial force.*

INTRODUCTION

Tube bending is a technique employed to fabricate components in numerous sectors, including aerospace, automotive, oil, and various other industries.

Numerous papers address the rotary draw bending process with various parameters; to elucidate this research, the following survey is proposed: B. Engel and H. Hassan [1], [2], [3], [4] determined the displacement of the neutral axis for various bending angles. The finite element simulation was compared with the findings of experimental tests. Furthermore, they analyzed the impact of several materials (Al alloy 6009 and stainless steel alloy 1.4547) on the rotary draw bending process. E. Daxin, Z. Guan, and J. Chen [5] derived a formula to determine the springback angle of a tube subjected to combined bending and extra stress, noting that the neutral layer shifts to the inner concave surface of the bend. N. Tang [6] investigated the plastic deformation in the bending of pipes and tubes. It also evolved to elucidate the phenomena in tube bending, with derivations for magnitudes such as stresses, wall thickness, shrinkage rate at the tube section, deviation of the neutral axis, feed preparation length of the bend, bending moment, and flattening.

D. Lue [7] the model incorporates non-linear strain-hardening and normal anisotropy under plane-strain conditions, including predictions of springback after unloading, the maximum bending moment at the bending limit, and the minimum bending radius. H. Al Qureshi A theoretical analysis of the elastic-plastic bending of a tube was offered. Analytical approaches are presented via which approximation equations are formulated to quantitatively predict springback behavior and residual stress distributions. J. Wang and R. Agarwal [8] The influence of axial force and internal

pressure was examined using plasticity theories and an analytical model constructed to predict cross-sectional deformation and thickness variation of tubes under various loading circumstances. H. Li, H. Yang, J. Yan, and M. Zhan [9] investigated wrinkling, wall thinning, and cross-sectional deformation, accompanied by an analytical description.

The deformation characteristics of thin-walled tubes under NC bending, with a large diameter-to-thickness ratio (D/t) ranging from 50.0 to 87.0 and a tiny bending radius-to-diameter ratio (Rd/D) between 1.0 and 2.0, are investigated by a set of robust 3D finite element models. Utilizing the ABAQUS platform. M. Zhan, H. Yang, Z. Jiang, Z. Zhao, and Y. Lin [10]developed a three-dimensional (3D) rigid-plastic finite element simulation system, TBS-3D (Tube Bending Simulation by 3D FEM), for the numerical control bending process of thin-walled tubes, based on the principles of the rigid-plastic finite element method (FEM), and established a coherent FEM model.

This finite element walled tube has been simulated, exhibiting distorted meshes at various bending stages. L. Sözen, M. Güler, D. Bekar, and E. Acar [11] A comprehensive research of the springback phenomenon was conducted, examining the interplay between geometrical and mechanical parameters rather than merely performing a one-at-a-time sensitivity analysis. This task is complete; surrogate models have been built utilizing data derived from finite element analysis conducted with the multi-purpose explicit and implicit finite element software Ls-DYNA to assess the non-linear response of structures.

I. Pahole, S. Bonifarti, M. Ficko, B. Vaupotic, S. Kovacic, and J. Balic The bending of sheet metal for angles over 90 degrees was examined using basic forming equipment [12]. The bending techniques known as "traktrix" (utilizing two steps) or "strip turning" (employing a single step) are applicable for executing intricate bends of 90 degrees or greater. J. Liu, H. Yang, M. Zhan, and Z. Jiang [13], [14], [15] have constructed a novel finite element model that incorporates the size-dependent effect. In modeling, the material properties derived from uniaxial tension and compression tests are applied to the outside and interior regions, respectively, and compared with experimental results.

This was compared with the prior analysis, which solely utilized tensile material parameters to assess prediction accuracies regarding the tube profile. The primary purpose of this study is to build an analytical model for calculating the tensile force based on the shifting of the neutral axis, alongside a finite element model of rotating draw bending that incorporates the effects of tensile force, which has been confirmed through experimentation. The influence of axial force on strain, wall thinning, wall thickening, and neutral axis displacement has been examined.

RESEARCH METHOD

A. Calculate the neutral axis shifting

The geometric configuration of the tube's cross-section and the tube post-bending are illustrated in Figure (1). The original neutral axis of the tube is located in the center

of the bending, and the distance from the tube's center to the bending die's center is referred to as the bending radius (Rb). All have been examined in prior research [2B].

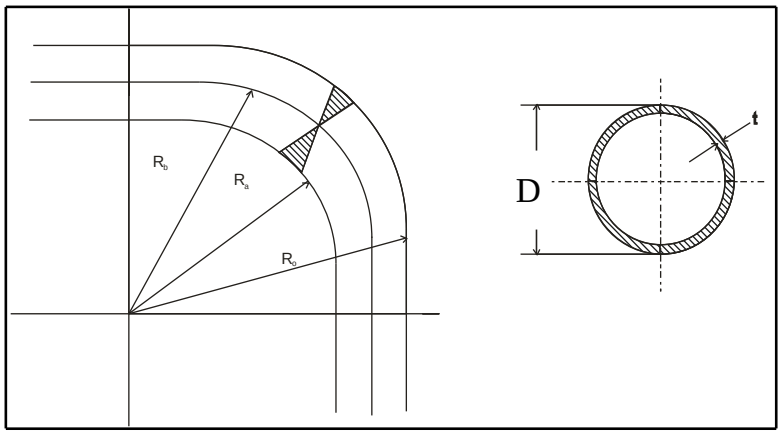

Figure 1. Rotary draw bending without tensile force.

This occurred without axial force; however, when axial force is applied, the neutral axis shifts to the inner arc of the tube shown in Figure (2).

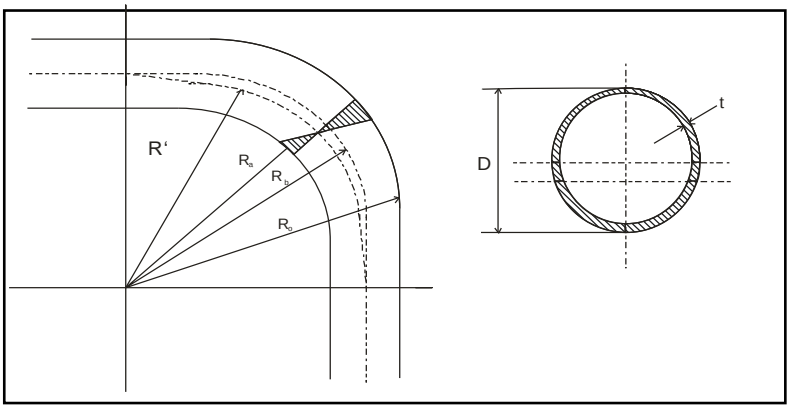

Figure 2. Rotary draw bending utilizing tensile force.

The greatest displacement of the neutral axis during tube bending is determined from the axial strain in the outer and inner arcs.

$$\mathrm{Ln}\left[\frac{R+r}{R\prime}\right] = -\mathrm{Ln}\left[\frac{R-r}{R\prime}\right] \quad (1)$$

$$R' = \sqrt{(R+r)(R-r)} \quad (2)$$

$$B = R / D \quad (3)$$

Where, B represents the bending factor, R denotes the bending radius, and r signifies the tube radius. Consequently, the practical tests indicate that the mathematical methods employed to derive formula number 4 for calculating the neutral axis shift are contingent upon the bending radius and bending factor, as illustrated in Figure 3.

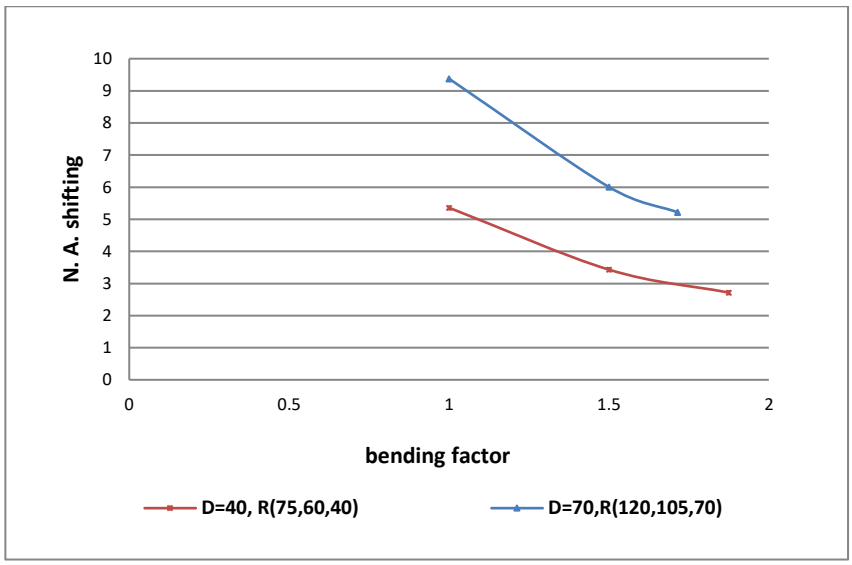

Figure 3. The neutral axis with deferent bending factor.

$Ne = 0.133*D*B^{(-1.083)}$ ……. (4).

Where D is the tube diameter, B is the bending factor, and e is the distance of the neutral axis. Additionally, equation (5) has been devised to account for the bending angle, as illustrated in Figure (4).

$ne = 0.18766*D*B*^{(-1.083)} * \sin \alpha$ …... (5).

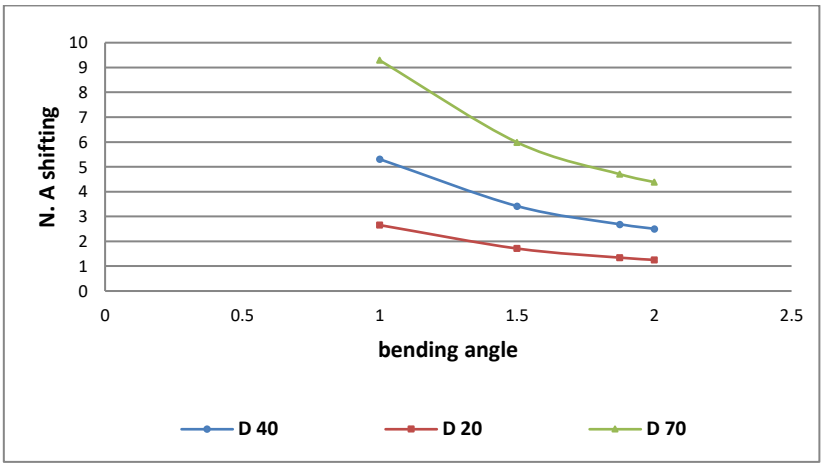

Figure 4. The neutral axis with deferent bending angle.

B. Calculate the axial force

In tube bending with axial force, the axial strain comprises two components: one resulting from tension (ϵxt), referred to as "the strain at the middle surface," and the other arising from bending [13], as illustrated in figure (5).

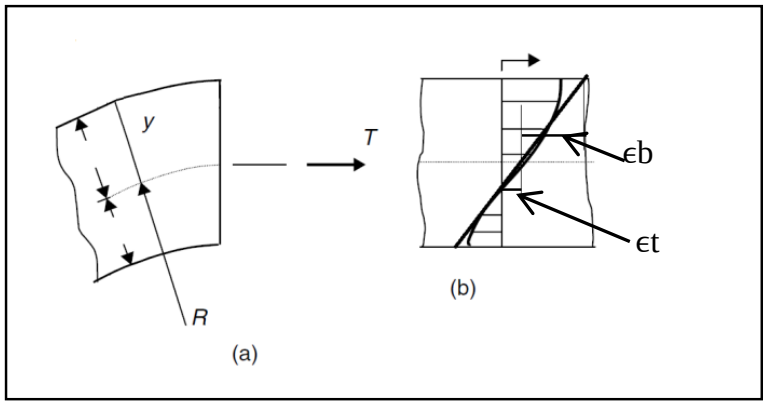

Figure 5. The distribution of strain in axial force rotary draw bending.

$\epsilon_\alpha = ln\,(\frac{L_s}{L_o}) + ln\,(1+\frac{y}{R})$

$\epsilon_\alpha = \epsilon_{\alpha t} + \epsilon_{\alpha b}$ ..... (6)

Where Lc=R*α ''the fiber in center of the tube'',
Lo=R *α ''the original length of the tube''.

e =R-R′

and

R′=R- e

A model for estimating the two-dimensional stress and strain in bent tube sections has been developed by N. Tang [6]. With a few assumptions, the yield stress is calculated using the same method. Additionally, a formula to determine the axial force based on neutral axis shifting, yield stress, wall thickness, and tube radius has been developed using the tension force formula for J. Wang and R. Agarwal [8].

$\epsilon_\alpha = \ln(1+e_\alpha)$ .....(7)

$\epsilon_c = \ln(1+e_c)$ .....(8)

$\epsilon_v = \ln(1+e_v)$ .....(9)

From von mises law

$\epsilon f = \sqrt{(2/3(\epsilon 1^2 + \epsilon 2^2 + \epsilon 3^2))}$ ..... (10)

Substituting eq. (4, 5, and 6) in eq. (7), we have

$\epsilon f = \frac{2}{\sqrt{3}}\sqrt{\epsilon 2\alpha + \epsilon c\epsilon\alpha + \epsilon c}$

And Ludwig law.

$Y = a\,\epsilon f^n$ ..... (11)

The axial force is given by

$F_t = \int_0^\beta Y * t * r sin\Phi d\Phi - \int_\beta^\pi Y * t * r sin\Phi d\Phi$ ..... (12)

Where Ft is the axial force, Y is the Yield stress, t is the wall thickness of the tube, r is tube radius and β= (90+θ) as shown in Figure (6).

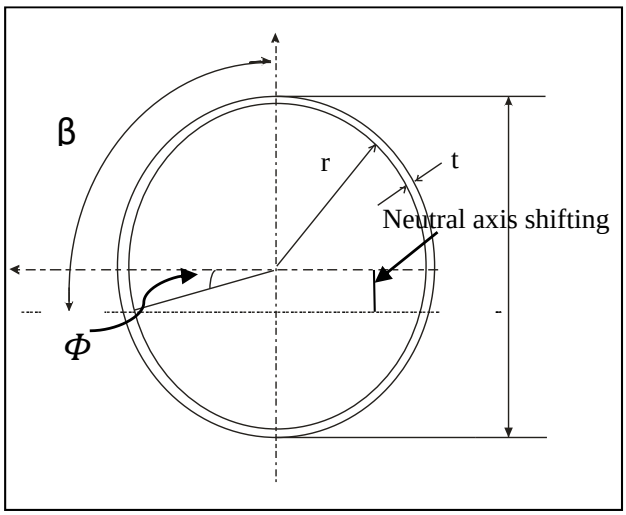

Figure 6. Displacement of the neutral axis as a result of applying axial force.

Finite Element Analysis

A finite element model of the tube bending process has been constructed for use with ABAQUS. The study employs finite element simulation to determine the wall thickness distribution of the tube's cross-section and the maximum strain distribution in all directions for the 1.4547 steel alloy. Figure 7 illustrates the finite element model for rotary draw bending, depicting both the pre-bending and post-bending states, including the meshing, bending die, clamp die, pressure die, wiper die, and the tension force applied to the tube.

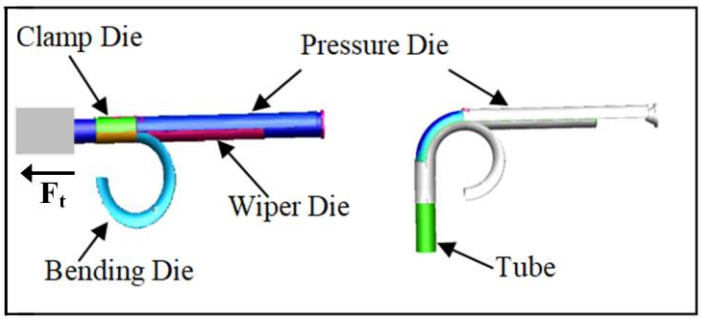

Figure 7. Finite element model for the rotary draw bending for tube with tension force.

The finite element simulation model was designed for use with axial force and all instruments, as illustrated in Figure 7. The ABAQUS program for tubes can perform simulations using axial force. This technique indicates that the neutral axis shifts to the inner arc of the bend during bending outcomes.

The strain distribution in the axial direction of the tube during rotating draw bending, both with and without tension, is illustrated in Figures 8 and 9. Additionally, the wall thickness distribution at the midpoint of bending, with and without axial force, is presented for a bending angle of 90°.

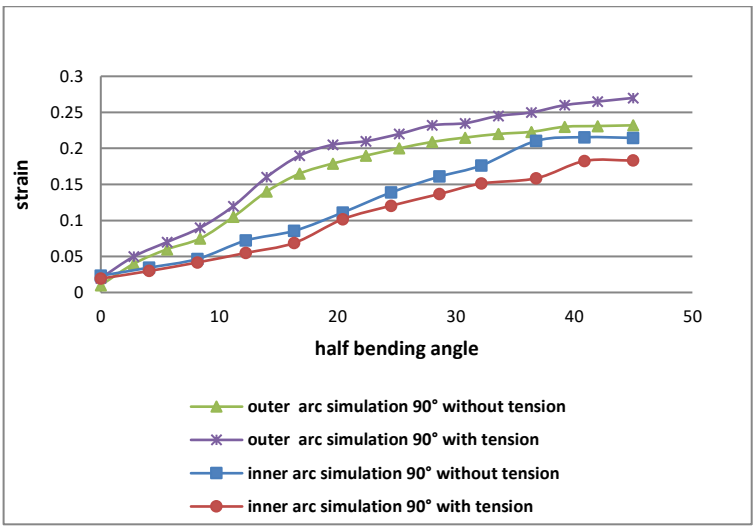

Figure 8. Impact of axial force on the distribution of axial strain within the tube.

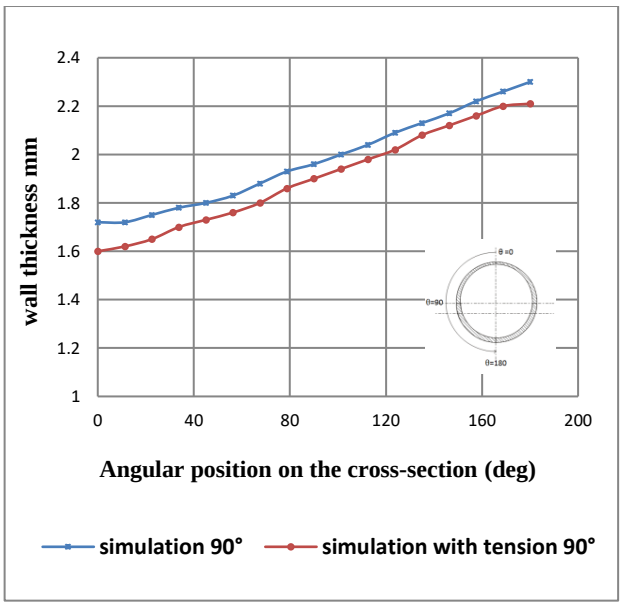

Figure 9. Distribution of wall thickness across the tube's cross-section.

Experimental

A. Rotary draw bending "with axial force and without axial force"

During the rotary draw bending operation, the tube is positioned within the bending machine and secured between the bend die and the clamp die. The rotation of both tools along the bending axis deforms the tube in accordance with the radius of the bend die, as seen in Figure 10. The pressure die (slide piece) functions to absorb the radial stress produced during the forming process and externally supports the straight tube end. The application of a mandrel and wiper die during mandrel bending can yield superior workpiece quality, especially for thin-walled tubes and tight bending radii.

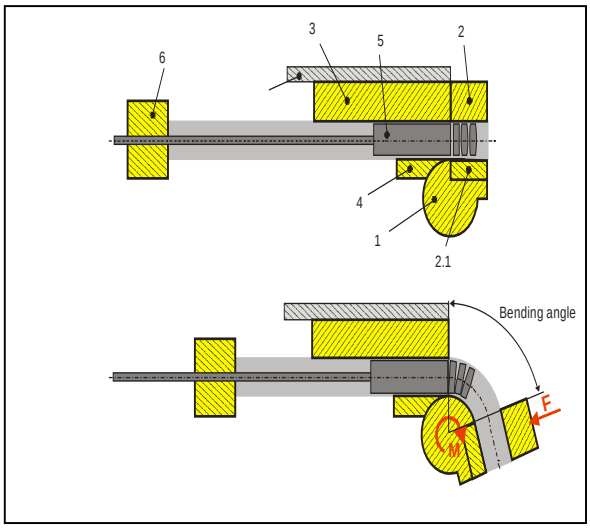

Figure 10. Tools for the rotary draw bending process.

The inner clamp die (2.1), outer clamp die (2), bend die (1), pressure die (3), wiper die (4), mandrel (5), and feed (6).

Rotary draw bending with axial force utilizes the same approach as rotary draw bending, but incorporates axial force on the tube, as seen in Figure (11).

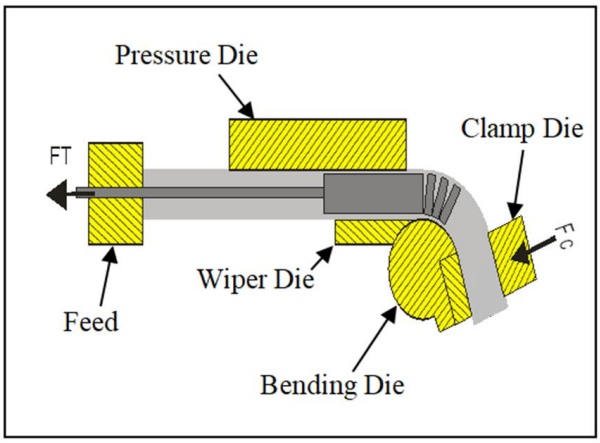

Figure 11. Rotary draw bending with clamp force Fc and Tension force Ft.

B. Material and experimental measurement

The study used a tube made from 1.4547 steel alloys. The initial external diameter, Do, is 40 mm, and the wall thickness is 2 mm. Figure 12 illustrates the flow curve of the tube material derived from tensile test analysis, compared with the Ludwik equation, Swift equation, and linear elastic plastic model. Table 1 delineates the mechanical parameters of the tube material.

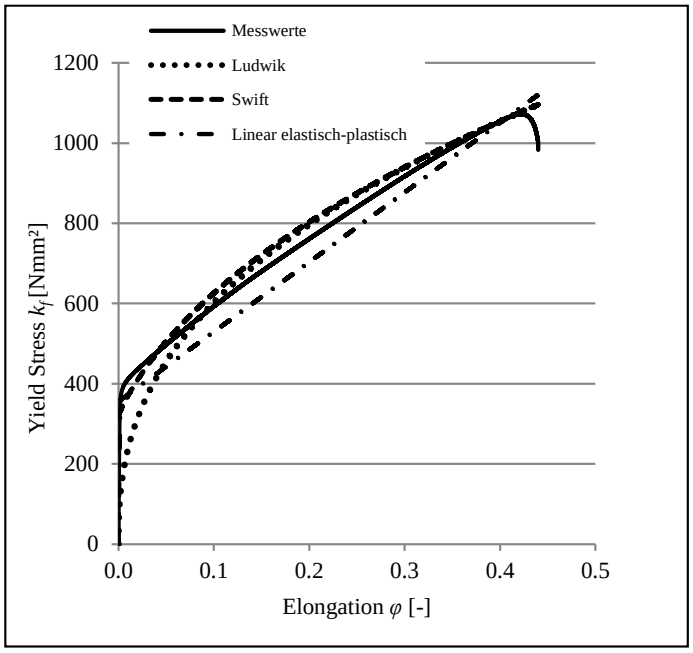

Figure 12. Yield stress-elongation for 1.4547 steel alloys.

Table 1. Mechanical parameters.

Parameter	Value
Density [g/cm³]	7.86
E-modul [Mpa]	210000
$R_{p0.2}$ [Mpa]	464.01
R_m [Mpa]	706.95
A_g [%]	44.68
Strength coefficient, K [Mpa]	1473.8
A 5,65	0.00
N [-]	3.694E-01

Strain measurement in the experimental test is conducted using a specialized software implemented via a specific technique.

The wall thickness measurement at the midpoint of the tube employs a wall thickness measuring equipment for high-resolution assessment of the tube wall thickness relative to its circumference. The apparatus comprises a caliper equipped with an inductive sensor. The sensor signal is quantified and transformed using a computer-integrated 16-bit A/D converter card. The high-resolution A/D converter offers a resolution of the electric field within the wall thickness of 0.6 µm, and with meticulous calibration, an absolute precision of about ±5 µm or more may be attained, as seen in Figure 15.

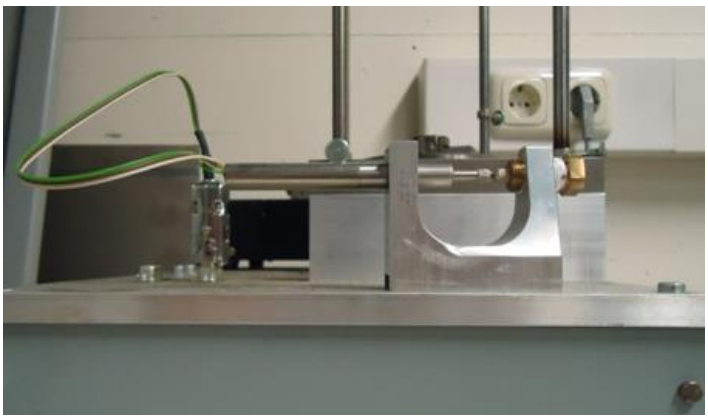

Figure 13. The instruments used for measuring wall thickness.

RESULTS AND DISCUSSION

A. Application of the axial force

The axial force was calculated as have been seen in section (2.2), were equation (4) calculated the force with different parameters and for material 1.4547 steel alloys. Figure (14) shows the results regarding the implementation of the axial force considering different parameters. Such as the following obtained result, which is an axial force 14 kN when the bending angle is 90°, bending radius 75 mm and the diameter 40 mm but the axial force equal to 9.83 kN when the bending angle is 45°, bending radius 75 and the diameter 40. And the result obtained is an axial force 34.49 kN when the bending angle is 90°, bending radius 105 mm and the diameter 70 mm but the axial force equal to 23.75 kN when the bending angle is 45°, bending radius 105 mm and the diameter 70mm.

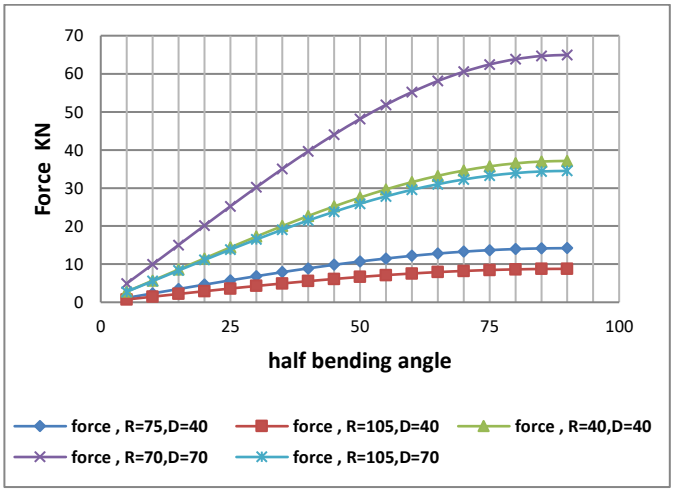

Figure 14. The axial force with deferent parameters.

B. Thickness distribution and neutral axis shifting

In this part, the axial force was applied during tube bending. The wall thicknesses are investigated by experimental and FE simulation results for bending with axial force and without axial force. The axial force 14.2 KN was applied at tube in the experimental and FE simulation to the bending angel 90°. Figure (14) shows the wall thickness distribution investigated by experimental and simulation in the middle of the tube. When

bending angle 90°, Hence outer arc fibres the minimum wall thickness in the tube with axial force (2.214mm) , (2.21mm) and without axial force (2.321mm),(2.3mm) investigated by experimental and FE simulation, respectively. The minimum wall thickness reductions at outer arc fibres were from (2.321mm) to (2.214mm) and (2.3mm) to (2.21mm) investigated by experimental and EF simulation result, respectively. Figure (14) also shows at the inner arc fibres the maximum wall thickness in the tube with axial force (1.465mm) (1.6mm) and without axial force (1.656mm) (1.72mm) investigated by experimental and FE simulation results, respectively. The maximum wall thickness reduction at inner arc fibres were from (1.656mm) to (1.465mm) and (1.72mm) to (1.6mm) investigated by experimental and FE simulation results, respectively.

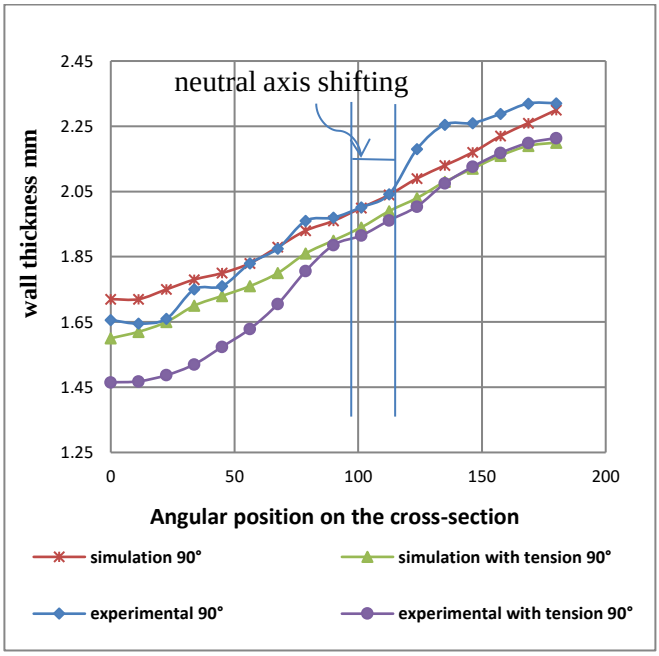

Figure 14. Comparison of wall thickness distribution on cross-section of the tube obtained from FE simulation and experimental results in the middle of bending ''without axial and without axial force'' (bending angle 90°).

As the wall thickness was variation with different bending angle. Figure (15) shows the wall thickness distribution investigated by experimental and simulation results at middle bending angle in the bending angle 45°, where in outer arc were (2.265mm)to (2.322mm) and (2.21mm) to (2.27mm) experimental with axial, experimental without axial, simulation with axial and simulation without axial, respectively. And in inner arc were (1.606mm) to (1.7mm) and (1.69mm) to (1.74mm) experimental with axial, experimental without axial, simulation with axial and simulation without axial, respectively.

In order to apply the axial force, the neutral axis was shifted ''see figure (14)'' where denoted the neutral axis shifting in rotary draw bending with axial force compared with RDB without axial force and as denoted the neutral axis shifting depend on the axial force and bending angle ''see figure (14&15)'' where the shifting in the neutral axis with

bending angle 90° more than the shifting in the neutral axis with bending angle 45° investigated by experimental and FE simulation.

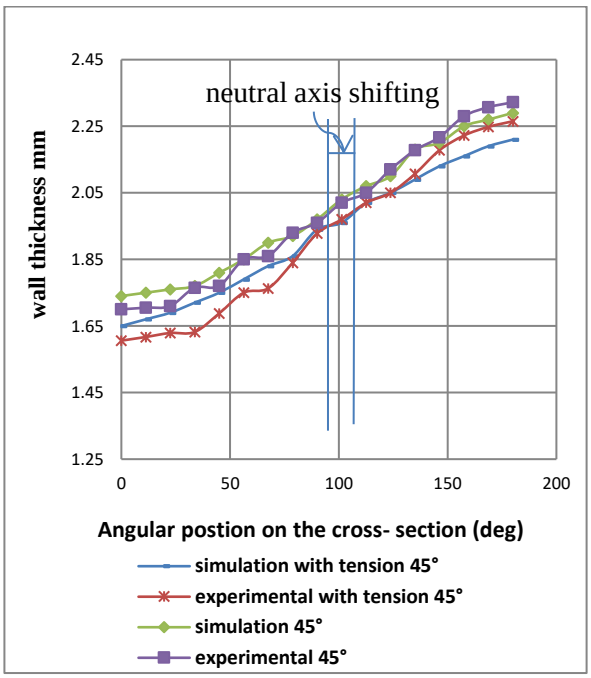

Figure 15. Comparison of wall thickness distribution on cross-section of the tube obtained from FE simulation and experimental results in the middle of bending ''without axial and without axial force'' (bending angle 45°).

C. Strain distribution

In this part, the strain distribution were investigated by experimental and FE simulation results. The axial effected predicted on the strain distribution results by experimental and FE simulation. Figure (16&17) shows the strain distribution in the outer arc were investigated at bending angle 90°, Hence the strain distribution in the half bending angle obtained with axial force (0.335), (0.27) and without axial force (0.27) (0.232) investigated by experimental and analytical results, respectively. The strain in the outer arc at half bending angle increased from (0.27) to (0.335) and from (0.232) to (0.27) investigated by experimental and FE simulation results, respectively. Figure (16&17) as shows the strain distribution but in inner arc for bending angle 90°, Hence the strain obtained at the half bending angle with axial force (0.159) (0.1831007) and without axial force (0.23) (0.214569) investigated by experimental and FE simulation results, respectively. The strain values reduction with axial force from (0.23) to (0.159) and from (0.214569) to (0.1831007) predicted by experimental and FE simulation results, respectively.

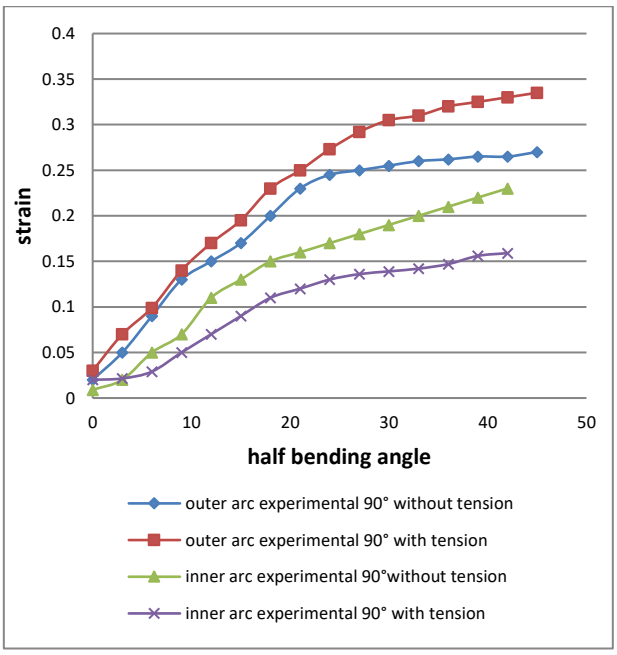

Figure 16. Effect of the axial force on the axial strain distribution of the tube ''from start to half bending angle'' obtained from experimental results (bending angle 90°).

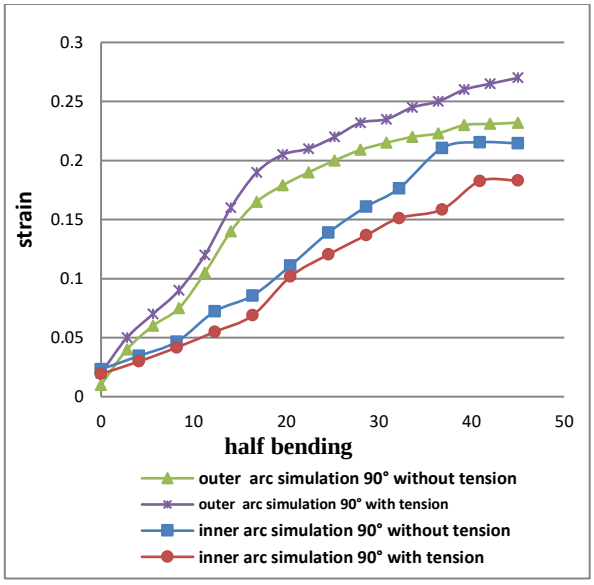

Figure 17. Effect of the axial force on the axial strain distribution of the tube ''from start to half bending angle'' obtained from FE simulation results (bending angle 90°).

As shown in Figure (18&19) the strain values changed with deferent bending angle, Hence the strain distribution investigated by experimental and FE simulation for bending angle 45° with axial force and without axial force. Where in outer arc were (0.281) to (0.23), (0.2109) to (0.19) and in inner arc (0.165) to (0.21), (0.1558637) to (0.187) investigated by experimental and FE simulation in half bending angle, respectively.

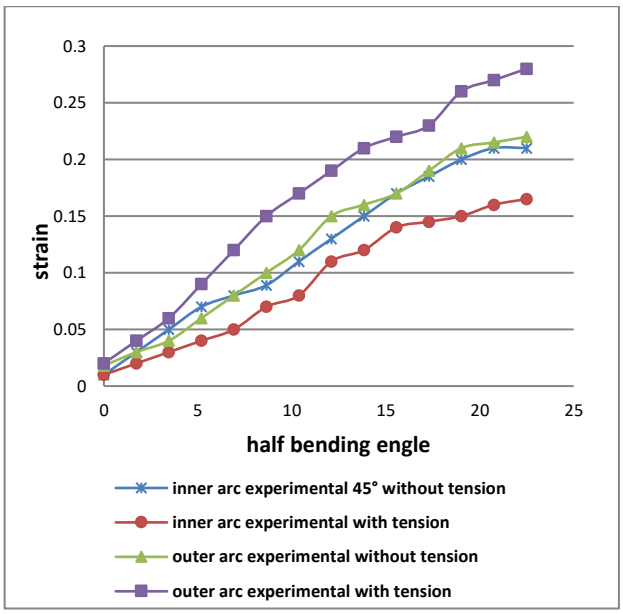

Figure 18. Effect of the axial force on the axial strain distribution of the tube ''from start to half bending angle'' obtained from experimental results (bending angle 45°).

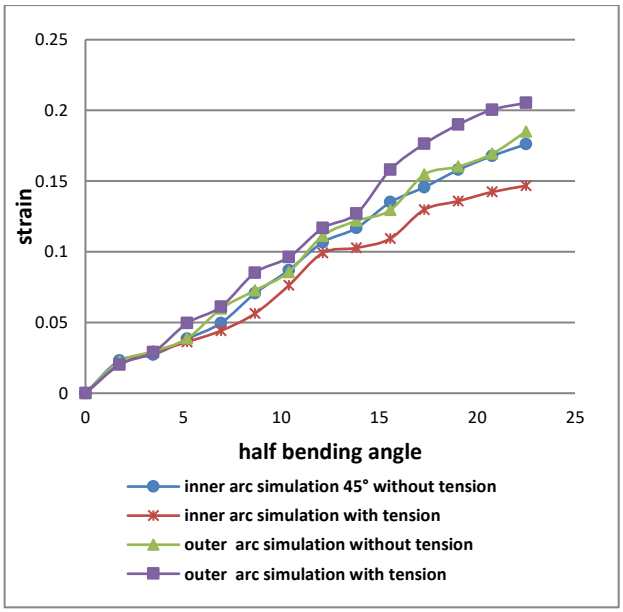

Figure 19. Effect of the axial force on the axial strain distribution of the tube ''from start to half bending angle'' obtained from FE simulation results (bending angle 45°).

CONCLUSION

Fundamental Finding : The study establishes a theoretical model to calculate axial force and confirms, through both experimental and finite element simulation, that axial force significantly affects tube bending behavior in the rotary draw bending process. **Implication :** Understanding how axial force influences strain distribution, wall thickness variation, and neutral axis shifting can help optimize tube bending parameters, leading to better product quality and manufacturing efficiency. **Limitation :** The conclusions are derived from specific tube geometries, materials, and bending parameters; results may

vary for other configurations or loading conditions not considered in this study. **Future Research :** Further investigations could explore axial force effects on different materials, tube diameters, and bending radii, as well as integrating real-time monitoring for adaptive process control.

REFERENCES

[1] B. Engel and H. Hassan, "Investigation of Neutral Axis Shifting in Rotary Draw Bending Processes for Tubes," *Steel Res. Int.*, vol. 85, 2014.

[2] H. R. Hassan, S. M. Abdulgaffar, K. K. Mohsen, and K. Egab, "Investigation of Material Properties Effect on the Ovalization Phenomenon in the Tube Bending Produced by RDB," in *IOP Conference Series: Materials Science and Engineering*, 2020, p. 12010.

[3] M. Altimemy, A. K. Ibrhim, H. R. Hassan, and M. J. Hayawi, "Computational Study of Pump Turbine Performance Operating at Off-Design Condition-Part I: Vortex Rope Dynamic Effects," *CFD Lett.*, vol. 17, no. 3, pp. 148–166, 2025.

[4] F. Cao, M. Al-Bahrani, D. A. Smait, N. Nasajpour-Esfahani, and M. Hekmatifar, "Effective parameters on the combustion performance of coated aluminum hydride nanoparticles: A molecular dynamics study," *Mater. Today Commun.*, vol. 36, p. 106586, 2023.

[5] E. Daxin, Z. Guan, and J. Chen, "Influence of addition tensile force on springback of tube under rotary draw bending," *J. Mater. Eng. Perform.*, 2012.

[6] N. Tang, "Plastic-deformation analysis in tube bending," *Int. J. Press. Vessel. Pip.*, vol. 77, pp. 751–759, 2000.

[7] D.-K. Leu, "A simplified approach for evaluating bendability and springback in plastic bending of anisotropic sheet metals," *J. Mater. Process. Technol.*, vol. 66, pp. 9–17, 1997.

[8] J. Wang and R. Agarwal, "Tube bending under axial force with internal pressure," in *ASME*, 2006.

[9] H. Li, H. Yang, J. Yan, and M. Zhan, "Numerical study on the deformation behaviors of thin-walled tube NC bending with large diameter and small bending radius," *Comput. Mater. Sci.*, vol. 45, pp. 921–934, 2009.

[10] M. Zhan, H. Yang, Z. Jiang, Z. Zhao, and Y. Lin, "A study on a 3D FE simulation method of the NC bending process of thin-walled tube," *J. Mater. Process. Technol.*, vol. 129, pp. 273–276, 2002.

[11] L. Sözen, M. Guler, D. Bekar, and E. Acar, "Investigation and prediction of springback in rotary-draw tube bending process using finite element method," *J. Mech. Eng. Sci.*, 2012.

[12] I. Pahole, S. Bonifarti, M. Ficko, B. Vaupotic, S. Kovacic, and J. Balic, "Bending of sheet metal of complicated shapes (for 90° angle and more) in combined tools," *J. Achiev. Mater. Manuf. Eng.*, vol. 16, no. 1–2, 2006.

[13] J. Liu, H. Yang, M. Zhan, and Z. Jiang, "Accurate prediction of the profile of thick-walled titanium alloy tube in rotary draw bending considering strength-differential effect," *Comput. Mater. Sci.*, vol. 60, pp. 113–122, 2012.

[14] H. Hasan, K. Egab, and H. Hassan, "Thermal and hydraulic characteristics study of different dimpled micro-channel heat sinks," in *AIP Conference Proceedings*, 2021, p. 80009.

[15] K. Egab, S. K. Oudah, A. A. Nassar, H. R. Hassan, and Y. Bhuiyan, "Investigation of temperature effect on cracked pressurized pipes," in *ASME International Mechanical Engineering Congress and Exposition, Proceedings (IMECE)*, 2018.

***Hassan Raheem Hassan (Corresponding Author)**
Al-Shatrah University, Iraq
Email: hassanraheem@shu.edu.iq